Journal of the Mechanical Behavior of Biomedical Materials 80 (2018) 143–154

Contents lists available at ScienceDirect

Journal of the Mechanical Behavior of Biomedical Materials

journal homepage: www.elsevier.com/locate/jmbbm

Improved tribocorrosion performance of bio-functionalized TiO_2 nanotubes under two-cycle sliding actions in artificial saliva

Sofia A. Alves[a,b,*], André L. Rossi[c], Ana R. Ribeiro[b,d,e], Fatih Toptan[a,f], Ana M. Pinto[a,f], Tolou Shokuhfar[g,h], Jean-Pierre Celis[i,j], Luís A. Rocha[a,b,k]

[a] CMEMS – Center of MicroElectroMechanical Systems, Department of Mechanical Engineering, University of Minho, Azurém, 4800-058 Guimarães, Portugal
[b] IBTN/BR – Brazilian Branch of the Institute of Biomaterials, Tribocorrosion and Nanomedicine, Faculty of Sciences, UNESP – Universidade Estadual Paulista, 17033-360 Bauru, SP, Brazil
[c] Brazilian Center for Research in Physics, 22290-180 Rio de Janeiro, RJ, Brazil
[d] Directory of Life Sciences Applied Metrology, National Institute of Metrology, Quality and Technology, 25250-020 Duque de Caxias, RJ, Brazil
[e] Postgraduate Program in Translational Biomedicine, University of Grande Rio, 25070-000 Duque de Caxias, RJ, Brazil
[f] Department of Mechanical Engineering, University of Minho, Azurém, 4800-058 Guimarães, Portugal
[g] Department of Bioengineering, University of Illinois at Chicago, 60607 Chicago, IL, USA
[h] IBTN/US – American Branch of the Institute of Biomaterials, Tribocorrosion and Nanomedicine, University of Illinois at Chicago, 60612 Chicago, IL, USA
[i] Department of Materials Engineering, KU Leuven, 3001 Leuven, Belgium
[j] Falex Tribology N.V., Wingepark 23B, 3110 Rotselaar, Belgium
[k] Faculdade de Ciências, Departamento de Física, UNESP – Universidade Estadual Paulista, 17033-360 Bauru, SP, Brazil

ARTICLE INFO

Keywords:
TiO_2 nanotubes
Bio-functionalization
Tribocorrosion
Two-cycle-sliding
Mechanical properties

ABSTRACT

After insertion into bone, dental implants may be subjected to tribocorrosive conditions resulting in the release of metallic ions and solid wear debris, which can induce to peri-implant inflammatory reactions accompanied by bone loss, and ultimately implant loosening. Despite the promising ability of TiO_2 nanotubes (NTs) to improve osseointegration and avoid infection-related failures, the understanding of their degradation under the simultaneous action of wear and corrosion (tribocorrosion) is still very limited. This study aims, for the first time, to study the tribocorrosion behavior of bio-functionalized TiO_2 NTs submitted to two-cycle sliding actions, and compare it with conventional TiO_2 NTs.

TiO_2 NTs grown by anodization were doped with bioactive elements, namely calcium (Ca), phosphorous (P), and zinc (Zn), through reverse polarization anodization treatments. Characterization techniques such as scanning electron microscopy (SEM), energy dispersive X-ray spectroscopy (EDS) and scanning transmission electron microscopy (STEM), were used to characterize the films. Tribocorrosion tests were carried out in artificial saliva (AS) by applying two cycles of reciprocating sliding actions. The open circuit potential (OCP) was monitored before, during, and after both cycles of sliding, during which the coefficient of friction (COF) was calculated. The resulting wear scars were analyzed by SEM and EDS, and wear volume measurements were performed by 2D profilometry. Finally, the mechanical features of TiO_2 NTs were accessed by nanoindentation.

The results show that bio-functionalized TiO_2 NTs display an enhanced tribocorrosion performance, ascribed to the growth of a nano-thick oxide film at Ti/TiO_2 NTs interface, which significantly increased their adhesion strength to the substrate and consequently their hardness. Furthermore, it was discovered that during tribo-electrochemical solicitations, the formation of a P-rich tribofilm takes place, which grants both electrochemical protection and resistance to mechanical wear. This study provides fundamental and new insights for the development of multifunctional TiO_2 NTs with long-term biomechanical stability and improved clinical outcomes.

1. Introduction

Metallic implants made out of titanium (Ti) and Ti-based materials are the most commonly used for dental implants therapies owing their mechanical properties, excellent biocompatibility and high corrosion resistance (Crawford et al., 2009; Zhang et al., 2013). However, these materials present serious shortcomings as regards the absence of osteogenesis inducing ability and the lack of antimicrobial properties (Crawford et al., 2009; Zhang et al., 2013; Zhao et al., 2011). To overcome these issues, various studies on the modification of Ti

* Corresponding author at: CMEMS – Center of MicroElectroMechanical Systems, Department of Mechanical Engineering, University of Minho, Azurém, 4800-058 Guimarães, Portugal.
E-mail address: sofiafonso@msn.com (S.A. Alves).

https://doi.org/10.1016/j.jmbbm.2018.01.038
Received 30 May 2017; Received in revised form 17 August 2017; Accepted 30 January 2018
Available online 01 February 2018

surfaces features such as morphology/topography and chemistry, have been undertaken (Zhang et al., 2013; Mendonça et al., 2011; Chen et al., 2013; Yazici et al., 2013; Holmberg et al., 2013; Arenas et al., 2013). A special focus has been devoted on the production of novel nanopatterned Ti implant surfaces, and at present, there is a strong believe that nano-functionalized surfaces will produce the new generation of dental implant materials (Mendonça et al., 2011; Tomsia et al., 2011; Puckett et al., 2010; Liu et al., 2010; Zhao et al., 2010).

In fact, nanotechnology is an emerging area in the field of dentistry, and the features of TiO_2 nanotubes (NTs) have been widely recognized as exceptional to promote osseointegration and reduce infection, the most commonly reported complications of currently used Ti-based dental implants (Crawford et al., 2009; Ercan et al., 2011; Popat et al., 2007a; Brammer et al., 2009; Shokuhfar et al., 2014). These are very flexible structures for building of new functionalities and further achieve enhanced biocompatibility (Vasilev et al., 2010). TiO_2 NTs may be easily coated with bioactive polymers (Gulati et al., 2012) or nanoparticles (Gao et al., 2014), and have demonstrated excellent ability to act as efficient and controlled drug delivery systems, by encapsulation of drugs, bioactive molecules or inorganic elements into their hollow cavities (Hu et al., 2012; Gulati et al., 2011; Popat et al., 2007b; Shokuhfar et al., 2013; Kodama et al., 2009). Furthermore, TiO_2 NTs have demonstrated ability to overcome the lack of biomechanical compatibility between metallic implants and bone. This is due to the lower elastic modulus that TiO_2 NTs display compared to Ti, and closer to that of natural bone, therefore avoiding stress shielding effect and consequently bone resorption (Crawford et al., 2009, 2007; Zhao et al., 2011; Rho et al., 1997; Soares et al., 2008).

Ti-based materials have a serious disadvantage since they are known to display low wear resistance (Budinski, 1991) and this may induce to various harmful consequences. During insertion, dental implants are subjected to both wear and corrosion actions (tribocorrosion) that may lead to material degradation *in vivo*. Furthermore, dental implants may be also exposed to tribocorrosion in a long-term, since cyclic micro-movements are known to take place at implant/bone interface as a consequence of transmitted loads during chewing action (Rodrigues et al., 2014; Szmukler-Moncler et al., 1998). Consequently, dental implant material degradation by wear-corrosion processes may result in the release of metallic ions and solid wear debris to adjacent tissues, which may induce to several biological complications (Rocha et al., 2013; Cruz et al., 2011; Olmedo et al., 2010). Various studies have shown that TiO_2 nanoparticles are internalized by bone cells impairing their functions (Ribeiro et al., 2016) and activating inflammatory reactions which may induce to osteolysis, and ultimately to implant failure (Cobelli et al., 2011; Ingham and Fisher, 2005, 2000). Therefore, the study of the degradation mechanisms of Ti and Ti-based materials by tribocorrosion mechanisms has been increasingly investigated over the past years (Sampaio et al., 2016; Toptan et al., 2016, 2017; Buciumeanu et al., 2017; Hacisalihoglu et al., 2015; Mathew et al., 2012; Souza et al., 2012, 2015; Villanueva et al., 2017; Cruz et al., 2015; Runa et al., 2013; Geringer and Macdonald, 2014; Sivakumar et al., 2011; Marques et al., 2016). However, despite the growing attention on the development of new implant systems based on TiO_2 nanotubular platforms, the study of their degradation behavior by tribocorrosion processes is still very limited in literature. To further emphasize this need, it has been reported that TiO_2 NTs display poor adhesion strength to the substrate (Miraghaei et al., 2011; Zhao et al., 2014; Yu et al., 2014) what might seriously compromise their widespread applications.

Recently, our group discovered reverse polarization anodization as a new functionalization technique of TiO_2 NTs, through which biocompatible TiO_2 NTs enriched with calcium (Ca) and phosphorous (P) were synthesized displaying superior corrosion behavior (Alves et al., 2017a). A step forward, our group produced TiO_2 NTs containing Ca and P, together with zinc (Zn), by the same technique, and provided a first insight on the bio-functionalization mechanisms of the nanotubular films (Alves et al., 2017b). One of the main outcomes of this previous study relies on the formation of a nano-thick oxide film at the interface of the NTs with the Ti substrate as a consequence of functionalization. Additionally, we have also recently found that the formation of that interfacial film significantly improved the tribocorrosion behavior of bio-functionalized TiO_2 NTs by increasing their adhesion strength to the Ti substrate (Alves et al., 2017c). Aiming to achieve further fundamental knowledge on this field, this contribution aims to study, for the first time, the tribocorrosion degradation behavior of bio-functionalized TiO_2 NTs when submitted to two- cycles of reciprocating sliding tests. These are intended to mimic the multiple mechanical solicitations that dental implants might be daily exposed. Here we describe the effect of bio-functionalization treatments on the tribocorrosion performance of TiO_2 NTs submitted to two-cycle sliding actions, and correlate it with the adhesion strength and mechanical properties of the films. This study brings novel insights on the degradation mechanisms of nanotubular systems highlighting the important role of bio-functionalization to construct structures with improved features, more feasible for future clinical applications.

2. Materials and methods

2.1. Synthesis of TiO_2 NTs and bio-functionalization

To prepare TiO_2 NTs, two anodization steps were carried out in an optimized organic electrolyte composed of ethylene glycol (EG, Fluka Analytical, St. Louis, MO, USA), 0.3 wt% ammonium fluoride (NH_4F, Ammonium Fluoride, Sigma-Aldrich, St. Louis, MO, USA) and 3 vol% distilled water. In the first anodization step Ti smooth samples (anode) were immersed in the EG-based electrolyte together with a graphite rod (cathode), separated at a distance of about 2 cm, and a constant voltage of 60 V was applied for 1 h. Afterwards, the resultant nanotubular film was intentionally removed by sonication in isopropanol (15 min) and distilled water (5 min), leaving a nanotextured Ti surface for the second anodizing step. The second anodization step was conducted at the previous conditions for an anodization time of 30 min, to synthesize vertically aligned and ordered TiO_2 nanotubular films with a specific morphology. The resulting Ti samples with TiO_2 NTs were named as NT.

Bio-functionalization of TiO_2 NTs was conducted based on a novel methodology described in previous works (Alves et al., 2017a, 2017b, 2017c), based on reverse polarization anodization treatments. The NT samples were subjected firstly to reverse polarization in an aqueous electrolyte composed of 0.35 M calcium acetate (Calcium acetate monohydrate, Sigma-Aldrich, St. Louis, MO, USA), 0.04 M β-glycerolphosphate (β-GP) (β-glycerolphosphate disodium salt pentahydrate, Sigma-Aldrich, St. Louis, MO, USA) and 0.35 M zinc acetate (Zinc acetate dihydrate, Sigma-Aldrich, St. Louis, MO, USA) as the source of calcium (Ca), phosphorous (P) and zinc (Zn), respectively. The reverse polarization step was carried out for 30 s in the Ca/P/Zn-based electrolyte, followed by anodization step in the same electrolyte for 30 min at 100 V. A graphite rod was used as the counter electrode and was placed about 2 cm away from the sample. After bio-functionalization, the nanotubular samples were named as NT-Ca/P/Zn. The outcomes of the tribocorrosion tests showed two dissimilar behaviors for these samples. Therefore, these were divided in two different groups named as NT-Ca/P/Zn#1 and NT-Ca/P/Zn#2.

NT, NT-Ca/P/Zn#1 and NT-Ca/P/Zn#2 samples, were cleaned in isopropanol (10 min), distilled water (5 min) and dried at room temperature. Finally, all the samples were stored in a desiccator until performing tribocorrosion tests.

A DC power supply (Keysight (Agilent) Technologies N5772A) was used for cathodic and anodic treatments with a limiting current of 2.5 A, and all of them were conducted at room temperature (22 – 24 °C) under stirring conditions.

2.2. Characterization of TiO_2 nanotubular films

The surface morphology of TiO_2 nanotubular samples was investigated before and after bio-functionalization treatments by scanning electron microscopy (SEM) using a FEI Helios NanoLab 650 equipped with a detector for energy dispersive X-ray spectroscopy (EDS). Elemental analyses of the samples were performed by EDS, using an acceleration voltage of 10 kV.

Thin cross-sections (around 100 nm thick) of TiO_2 nanotubular films were obtained by a dual beam instrument equipped with focused ion beam (FIB) with a gallium (Ga) ion source (TESCAN, LYRA 3). A platinum (Pt) layer of 1 μm was deposited *in situ* using a gas injection system and 1 nA Ga^+ ion current accelerated at 30 kV aiming to protect the thin cross-sections. The initial etching was conducted with 5 and 2 nA at 30 keV, and thinning was performed in 4 steps to obtain a lamella of ~ 100 nm: 1) 1 nA/30 keV; 2) 0.1 nA/10 keV; 3) 10 pA/5 keV; and 4) ~ 5 pA/3 keV. The Ti/TiO_2 NTs interface was observed by imaging the FIB-sections by dark-field scanning transmission electron microscopy (STEM-DF) using a JEOL 2100 F operating at an accelerating voltage of 200 kV.

2.3. Tribocorrosion experiments

A tribo-electrochemical approach was used to investigate the degradation behavior of nanotubular samples under the simultaneous action of wear and corrosion. The samples were fixed in an electrochemical cell, with an exposed surface area of 0.63 cm^2 to the test solution. A modified Fusayama's artificial saliva (AS) (Fusayama et al., 1963) was used at 37 °C (pH = 5.5), with chemical composition as follows: NaCl (0.4 g/L), KCl (0.4 g/L), $CaCl_2{\cdot}2H_2O$ (0.795 g/L), $Na_2S{\cdot}9H_2O$ (0.005 g/L), $NaH_2PO_4{\cdot}2H_2O$ (0.69 g/L) and Urea (1 g/L). This solution has been previously used in various studies (Souza et al., 2012; Alves et al., 2014, 2015; Robin and Meirelis, 2007) to mimic the extremely corrosive oral environment composed of Cl^-, F^-, and H^+ ions, which play a significant role on corrosion of dental implant materials (Souza et al., 2015). Furthermore, it is known that metallic materials display a similar electrochemical behavior in Fusayama´s saliva and natural saliva (Holland, 1992). Tribocorrosion experiments were conducted in a pin-on-disk CETR tribometer (Model UMT 2, Campbell, California, USA) with a reciprocating sliding configuration, and an alumina (Al_2O_3) ball (Ø 10 mm) was used as the counterbody. The tests were carried out using a three-electrode setup with testing samples as the working electrode, a platinum counter electrode, and a saturated calomel electrode (SCE) (Hg/Hg_2Cl_2/saturated KCl solution; SCE = +244 mV *vs.* NHE) was used as the reference electrode.

Before mechanical solicitations, the open circuit potential (OCP) was monitored using a potentiostat Gamry Reference 600 coupled to Gamry framework software (Gamry Instruments, Warminster, PA, USA) until stabilization. Afterwards, OCP measurements were conducted during two independent cycles of reciprocating sliding as well as after each period of mechanical solicitations. Each cycle of sliding lasted 1800 s followed by a period of OCP stabilization of 2000 s. To imitate the stresses and movements generated during masticatory action, reciprocating sliding tests were carried out at a normal load of 1 N (initial Hertzian contact pressure of 400 MPa) and a sliding frequency of 1 Hz (Mathew et al., 2012; Butt et al., 2015). Two independent cycles of sliding were carried out for 1800 s aiming to simulate the multiple periods of mechanical solicitations that dental implants might be daily exposed during mastication activity (Mathew et al., 2012; Butt et al., 2015). Moreover, to mimic the micro-movements generated at implant-bone interface as a result of the transmitted mastication loads, a linear displacement amplitude of 650 μm was selected (Cruz et al., 2011; Butt et al., 2015). During both periods of sliding the tribometer was coupled to UMT-2 software (Campbell, California, USA) to monitor the tangential force during sliding, through which the coefficient of friction (COF) was calculated. At the end, all the samples were ultrasonically cleaned with isopropanol (10 min) followed by distilled water (5 min), and lastly dried at room temperature. To assure the repeatability of the results, all the tests were accomplished for a minimum number of three samples for each group.

2.4. Characterization of the wear tracks

After tribocorrosion testing, the morphological and chemical features of the wear scars were investigated by SEM (FEI Nova 200 (FEG/SEM)) and EDS (Pegasus X4M).

To calculate the wear volume of the samples, the model previously described by Doni et al. (2013) was strictly followed. The wear track length was taken constant for all the tests as 650 μm. The width and the deepness of the wear tracks were extracted from the profiles obtained by 2D profilometry (Veeco, Dektak 150) and the data analysis was performed with the software (Dektak version 9.4). The final wear volume measurements were calculated from three wear tracks for each condition of test.

2.5. Nanoindentation tests

The mechanical properties of Ti polished samples (mirror-finishing) and TiO_2 nanotubular samples were measured using a nanoindentation system (Micro Materials NanoTest), with a load resolution of 50 nN.

To avoid the influence of substrate, preliminary experiments were carried out to select the most appropriate load to be applied, in such a way that the maximum indentation depth was always less than 10% of the thickness of the films (Soares et al., 2008). Afterwards, the maximum applied load during nanoindentation was set as 5 mN and the holding time was 5 s.

The reduced modulus (E_r) and hardness were determined from indentation load-displacement data following the Oliver and Pharr methodology (Oliver and Pharr, 1992). The hardness is determined from the maximum load and the projected area of contact. The E_r combines the mechanical properties of the indenter and the sample, and is given by the following equation:

$$\frac{1}{E_r} = \frac{(1-\nu_1^2)}{E_1} + \frac{(1-\nu_2^2)}{E_2} \quad (1)$$

where ν_1 and E_1 are the Poisson´s ratio and Young's modulus of the specimen and, ν_2 and E_2 are the Poisson's ratio and Young's modulus of the indenter, respectively. For the diamond Berkovich indenter probe used, E_2 = 1140 GPa and ν_2 = 0.07. The ν_1 of TiO_2 NTs was chosen to be the same as that bulk TiO_2 (*i.e.* 0.28) (Xu et al., 2015), while the ν_1 of Ti was assumed as 0.32. The elastic modulus (E) of TiO_2 NTs and Ti samples was calculated by fitting the measured E_r values in Eq. (1). The minimum of six indentations per each sample were used for elastic modulus and hardness calculations.

2.6. Statistical analysis

In this study the data is presented as the arithmetic mean ± standard deviation (SD). The statistical analysis was conducted by means of statistical tool SigmaStat 3.5 (Systat Software, San Jose, CA, USA). Data analysis was performed by one-way analysis of variance (ANOVA) in combination with Tukey HSD post hoc test, with a significance level of $p < .05$.

3. Results

3.1. Characterization of TiO_2 nanotubular films

The surface morphology of TiO_2 NTs synthesized by two-step anodization of titanium (Ti) surfaces is shown in Fig. 1a. After bio-functionalization of NT samples in the Ca/P/Zn-based electrolyte by reverse polarization and anodization processes, the morphology of the NTs was

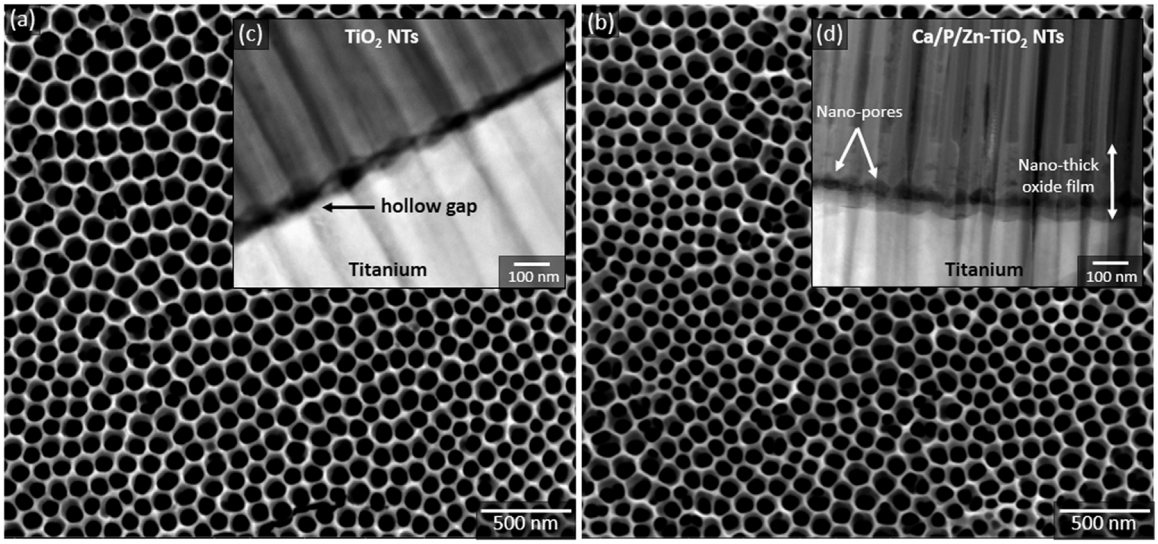

Fig. 1. SE SEM micrographs of (a) NT and (b) NT-Ca/P/Zn surfaces. Dark-field STEM micrographs at the interface of (c) NT and (d) NT-Ca/P/Zn nanotubular films. In (c) the inset white arrow shows the lacuna between Ti substrate and NT film while in (d) shows the nano porosity at the interface as well as the nano-thick oxide film grown during bio-functionalization (230 – 250 nm).

Table 1
Atomic percentage (at%) of the elements detected in NT and NT-Ca/P/Zn samples by EDS.

Element	NT (at% ± SD)	NT-Ca/P/Zn (at% ± SD)
Ti K	21.82 ± 1.64	23.66 ± 1.05
O K	53.18 ± 1.26	51.70 ± 3.98
F K	8.90 ± 0.53	9.46 ± 0.73
Ca K	–	0.26 ± 0.04
P K	–	0.33 ± 0.03
Zn L	–	1.35 ± 0.12

preserved as shown in Fig. 1b. Both nanotubular surfaces are characterized by NTs with non-uniform diameters ranging from 50 to 90 nm as reported in our previous study (Alves et al., 2017a). The chemical features of NT and NT-Ca/P/Zn samples were determined by semi-quantitative EDS analysis, and the atomic % of the elements detected is depicted in Table 1. Both groups of samples are composed of Ti, oxygen (O) and fluorine (F), and NT-Ca/P/Zn samples are additionally constituted of Ca, P and Zn elements. In a previous work, XPS studies conducted in NT samples showed that Ti and O were mainly found as TiO_2 (Alves et al., 2017a). Furthermore, the successful incorporation of Ca, P and Zn in TiO_2 NTs by reverse polarization anodization has been already achieved and described in a previous study of our group, in which these elements were found uniformly distributed along the topmost regions of the nanotubular films as well as along their length (Alves et al., 2017b).

The interfacial features of TiO_2 nanotubular films were studied before and after bio-functionalization treatments. Although no differences were found on NTs morphology, bio-functionalization induced to significant changes at the interface between the Ti substrate and TiO_2 NTs, which is shown in Fig. 1c and d for NT and NT-Ca/P/Zn samples respectively. For conventional TiO_2 NTs, a hollow space is found between the Ti substrate and TiO_2 NTs (Fig. 1c), suggesting a poor adhesion strength of the NTs to the substrate. On the other hand, after bio-functionalization treatments, the hollow gap existing before display different features due to the formation of a nano-thick oxide film with thickness comprised between 230 and 250 nm (Fig. 1d). This newly formed film at the interface, despite present some porosity at the nanoscale range, induced the formation of a more continuous interface which appears to improve the adhesion of the film to the Ti substrate. As recently reported by our group, this interfacial film is also constituted by Ca, P and Zn elements as a consequence of bio-functionalization treatments (Alves et al., 2017b).

3.2. Tribocorrosion behavior of TiO_2 nanotubular films submitted to two-cycle sliding tests

3.2.1. Open circuit potential and coefficient of friction evolutions

The open circuit potential (OCP) evolution before two-cycle sliding tests on NT and NT-Ca/P/Zn samples is shown in Fig. 2a. It is noteworthy that two different trends were observed during sliding tests carried out in NT-Ca/P/Zn samples and both trends are reported as NT-Ca/P/Zn#1 and NT-Ca/P/Zn#2. Before mechanical solicitations, all the samples were immersed in artificial saliva (AS) until OCP stabilization. The OCP reflects the electrochemical surface activation stage (active *vs.* passive), revealing its tendency to corrosion so that a higher OCP indicates a lower corrosion trend. After the period of stabilization both group of samples stabilized at significantly different OCP values. NT samples achieved a stable OCP around −0.14 V *vs.* SCE that differs strikingly from NT-Ca/P/Zn samples potential, which stabilized around 0.11–0.12 V *vs.* SCE. Higher OCP values were found for NT-Ca/P/Zn samples as compared to NT samples during the whole duration of two-cycle sliding tests. These differences might be related with the different interfacial features of TiO_2 nanotubular films before and after bio-functionalization treatments, as will be further on discussed in more detail (Section 4).

As soon as the first cycle of sliding starts on NT samples (SLIDING 1), it is observed that the OCP is kept stable for approximately 100 s and afterwards, a gradual decrease takes place during its whole duration reaching the lowest value of −0.3 V *vs.* SCE. As soon as the sliding is finished the OCP gradually evolves to noble values during the whole 2000 s stabilization period. Once the second cycle of sliding starts (SLIDING 2), the OCP starts to decrease immediately and a gradual lowering is observed during its complete duration reaching a minimum value of −0.3 V *vs.* SCE. Interestingly, it is noticed that after the end of SLIDING 2, the OCP tends to stabilize at a value similar to that achieved previously in the final stage of SLIDING 1. The coefficient of friction (COF) evolution during SLIDING 1 is shown in Fig. 2b. It is observed that in the first period of 300 s of sliding the COF is around 0.7–0.75, and after this period it decreases and tends to stabilize in values around 0.66–0.67. As observed in Fig. 2c, once the SLIDING 2 starts, the COF values are similar to the ones measured at the end of SLIDING 1 (*i.e.* 0.66–0.67) and these slightly drop down during SLIDING 2, reaching a

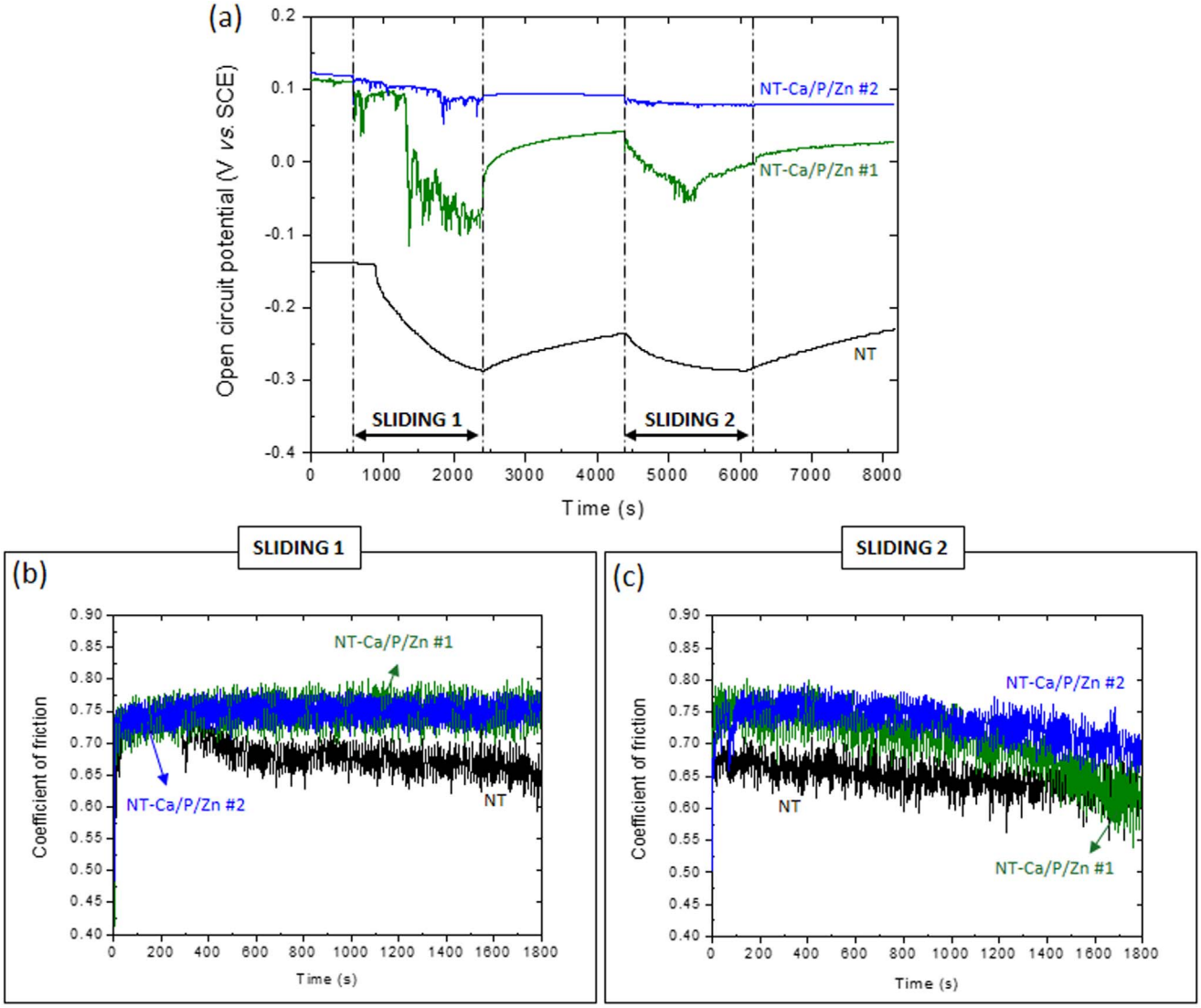

Fig. 2. (a) Evolution of the open circuit potential (OCP) before, during and after two-cycle reciprocating sliding tests in NT, NT-Ca/P/Zn#1 and NT-Ca/P/Zn#2 samples. The coefficient of friction values (COF) measured during the first sliding cycle (SLIDING 1) are shown in (b), while in (c) are depicted the COF values registered during the second sliding cycle (SLIDING 2). Both sliding periods lasted for 1800 s. (For interpretation of the references to color in this figure, the reader is referred to the web version of this article.)

minimum value of around 0.61 at the final stage.

As referred above, two distinct electrochemical behaviors were observed for NT-Ca/P/Zn samples submitted to two-cycle sliding tests and both are presented in Fig. 2a as NT-Ca/P/Zn#1 and NT-Ca/P/Zn#2. As soon as the first cycle of mechanical solicitations starts on NT-Ca/P/Zn#1 samples, the OCP immediately drops a few mV and is maintained stable during approximately 800 s. After this time, the OCP drops until −0.1 V *vs.* SCE and immediately after goes up again, and then tends to slightly progress to lower values until SLIDING 1 is stopped, reaching a minimum value of 0.08 V *vs.* SCE. At the end of SLIDING 1 the OCP immediately and rapidly evolves to higher values, and after 2000 s stabilize at around 0.04 V *vs.* SCE. After the period of stabilization when the second cycle of sliding starts, the OPC falls down and gradually reaches lower values during approximately 1000 s, after which the OCP starts to evolve to values increasingly high. As soon as SLIDING 2 is stopped, the OCP increases and reaches a similar value to the one initially recorded before the second sliding action. Concerning the COF evolution during SLIDING 1, this is maintained in a stable value of 0.75 during its total duration. When SLIDING 2 starts the COF is similar to the one attained at the end of SLIDING 1, and it slowly falls to lower values during the whole duration of mechanical solicitations. However, a remarkable higher drop is observed after 1000 s of sliding, which is coincident with the moment at which the OCP starts to increase (Fig. 2a).

In respect to NT-Ca/P/Zn#2 samples, as soon as SLIDING 1 starts the OCP drops only a few millivolts (around 0.01 V *vs.* SCE) and reaches a steady state for approximately 1200 s, after which the OCP falls down again a few millivolts and remain stable until the end of sliding. Once it is finished, the OCP evolves to more noble values reaching a stable value similar to the one achieved during the first plateau. After 2000 s stabilization period, the SLIDING 2 starts and the OCP slightly drops a few millivolts, and is maintained stable during the whole duration of sliding. Once mechanical action is finished, the OCP recovers and stabilizes in a value about 0.01 V *vs.* SCE, slightly inferior to the one recorded immediately before SLIDING 2. The COF evolution during the first cycle of sliding is similar to the one observed for NT-Ca/P/Zn#1 samples, which was kept in a stable value of 0.75. During SLIDING 2 duration, the COF measured is similar to the one registered at the end of SLIDING 1 and starts slowly decreasing after about 1000 s, which is coincident with the moment that COF values start decreasing for NT-Ca/P/Zn#1 during SLIDING 2 (Fig. 2c). It is noteworthy that the COF values measured during all the cycles indicate the presence of Ti oxide in the contact region, as they are in accordance with the ones previously reported in literature for similar Ti oxide/alumina tribological pairs

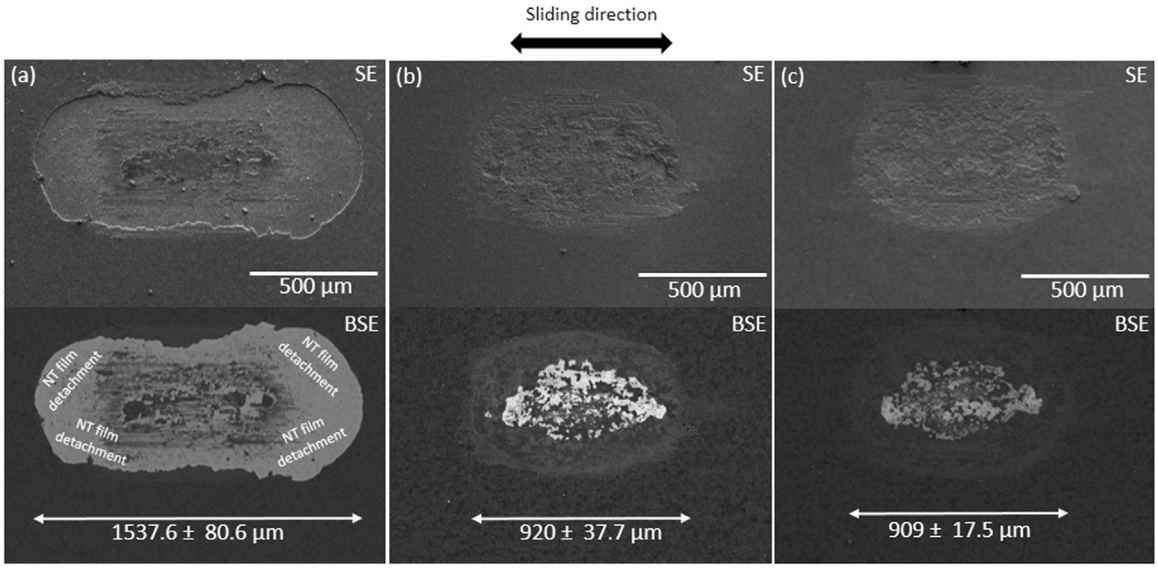

Fig. 3. SE/BSE SEM micrographs of the wear tracks in (a) NT, (b) NT-Ca/P/Zn#1 and (c) NT-Ca/P/Zn#2 samples after two-cycle reciprocating sliding tests in artificial saliva. The maximum wear tracks length is included in BSE images for all the groups.

(Alves et al., 2017c, 2014, 2015, 2013).

3.2.2. Wear tracks characterization

Representative SEM images of the wear tracks on NT, NT-Ca/P/Zn#1 and NT-Ca/P/Zn#2 samples are shown in Fig. 3. The SEM images are shown both in secondary electron (SE) and backscattered (BSE) imaging modes aiming a better characterization of the topographical and chemical features of the worn areas resulting from two-cycle reciprocating sliding tests.

From SE/BSE SEM images of the wear track on NT samples (Fig. 3a) it is observed that TiO_2 nanotubular film detached from the Ti substrate, including from the periphery of the sliding contact area. Film detachment is transduced in a wear track with irregular borders and a significantly higher length when compared to the wear tracks on NT-Ca/P/Zn#1 (Fig. 3b) and NT-Ca/P/Zn#2 (Fig. 3c) samples. The brighter areas in BSE SEM images are related to those regions characterized by a high atomic number, namely Ti, and contrast with those darker areas where elements with a low atomic number are present, such as O. In this light is it observed that the central region of the wear track of NT samples is characterized by the presence of oxidized areas, which are probably related to the formation of a tribofilm as a consequence of oxide film debris entrapment and compactness in the contact region. In contrast, both wear tracks on NT-Ca/P/Zn samples are characterized by curved borders with similar dimensions, and the detachment of the nanotubular film seems that have occurred mainly in the central region of the wear tracks, as suggested by the brighter contrast in BSE images (Fig. 3b and c).

A more detailed view of the wear tracks in the border and central regions is provided by BSE SEM images shown in Fig. 4a and b for NT samples. From these images it is confirmed that the film has been completely detached from the periphery of the contact region with Ti substrate becoming exposed to the aggressive environment provided by AS, and cracks are observed in the film remaining outside the wear track. In the central region, the presence of areas from where the nanotubular film was detached are observed, along with others where the formation of a compact oxide film took place (tribofilm). The presence of the Ti oxide tribofilm was confirmed through the detection of Ti and O by EDS analysis (results not shown).

No significant differences were observed in the border and central regions of the wear tracks on NT-Ca/P/Zn#1 and NT-Ca/P/Zn#2 samples, and the representative images of their wear tracks are shown in Fig. 4c (border) and Fig. 4d (center). In the border region it is observed that the film is characterized by areas with dissimilar levels of damage: smoother areas that contrast with rougher regions with pores obstructed, and others where open tubes are still visible. In the central region, it is confirmed that NTs have been completely detached in some areas, while in others still maintain their integrity. The obstruction of the pores in the topmost regions is also observed and indicated in Fig. 4d.

3.2.3. Wear volume

After two-cycle sliding tests, wear volume measurements were performed by 2D profilometry. The final wear volumes include both the contribution of wear due to corrosion and sliding wear, and are graphically presented in Fig. 5. The wear volume loss in conventional TiO_2 nanotubular samples was $4.05 \pm 1.24 \times 10^6$ µm^3, significantly higher as compared to NT-Ca/P/Zn#1 and NT-Ca/P/Zn#2 samples whose wear volumes were measured as $1.22 \pm 0.01 \times 10^6$ µm^3 and $1.58 \pm 0.22 \times 10^6$ µm^3 respectively.

3.3. Mechanical properties of TiO_2 nanotubular films

The mechanical properties of TiO_2 nanotubular films were accessed before and after bio-functionalization treatments. An additional group of samples of pure Ti was included due to its relevance on clinical procedures in respect to dental implants. The elastic modulus and the hardness of Ti, NT and NT-Ca/P/Zn samples are depicted in Table 2.

TiO_2 NTs revealed a significantly lower elastic modulus when compared to pure Ti samples, both before and after bio-functionalization. As regards hardness measurements, Ti samples displayed significantly higher values in relation to both NT and NT-Ca/P/Zn samples. Interestingly, after bio-functionalization treatments an increase in the hardness of the nanotubular films is observed, as shown by the significantly higher hardness measured for NT-Ca/P/Zn as compared to NT samples (Table 2).

4. Discussion

4.1. Tribocorrosion degradation of TiO_2 nanotubular films under two-cycle sliding tests

The understanding of how new implant surfaces behave when submitted to the simultaneous action of sliding wear and corrosion is of paramount importance since dental implants might be exposed to these

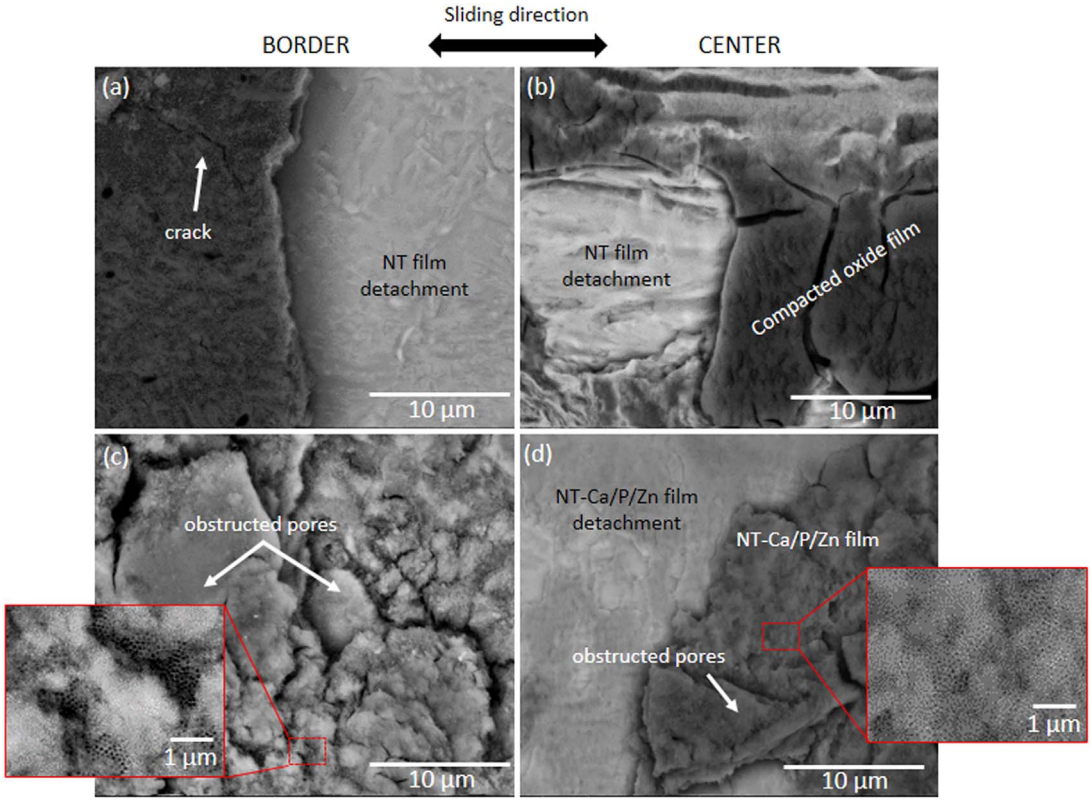

Fig. 4. BSE SEM micrographs of the wear tracks of (a and b) NT; (c and d) NT-Ca/P/Zn samples in the border and central regions. The inset images in (c) and (d) show the presence of TiO_2 NTs in the border and central regions.

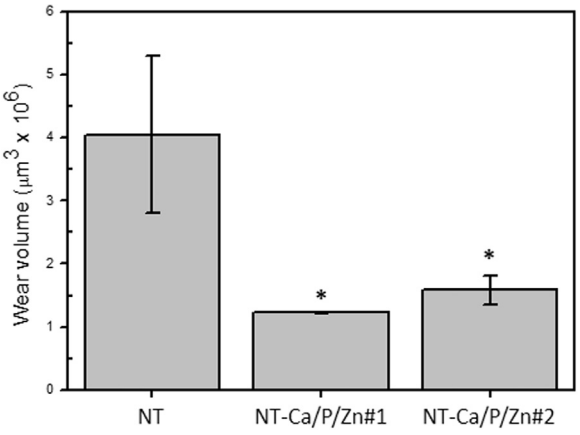

Fig. 5. Wear volume measurements after two-cycle reciprocating sliding tests in NT, NT-Ca/P/Zn#1 and NT-Ca/P/Zn#2 samples. (*) significantly different from NT, $p < .05$.

Table 2
Elastic modulus and hardness values measured for Ti, NT and NT-Ca/P/Zn samples.

Group	Elastic modulus (GPa ± SD)	Hardness (GPa ± SD)
Ti	127.25 ± 5.80	2.58 ± 0.12
NT	46.18 ± 4.03*	0.58 ± 0.08*
NT-Ca/P/Zn	46.99 ± 4.05*	0.89 ± 0.15*,#

* Significantly different from Ti, $p < .05$.
\# Significantly different from NT, $p < .05$.

actions at early, mid and long-term after insertion. Relative micro-movements take place between the implant surface and the surrounding bone tissue and may lead to several and harmful complications. In our present contribution we report on the synthesis of novel bio-functionalized TiO_2 nanotubular surfaces and their tribocorrosion performance. To simulate the multiple periods of mechanical solicitations that dental implants might be daily exposed when *in vivo* conditions, bio-functionalized TiO_2 NTs were submitted to two-cycle sliding actions in the presence of artificial saliva (AS) and their tribocorrosion response was compared with conventional TiO_2 NTs.

After immersion of NT samples in AS a stable OCP is achieved (Fig. 2a – black curve) and once SLIDING 1 takes place it is kept stable for 100 s, followed by a gradual decrease during the whole duration of sliding. Variations in OCP reflect the passive or active electrochemical state of the material. An increase (anodic shift) indicates a more passive state while a decrease (cathodic shift) suggests a more active state (Ponthiaux et al., 2004). Furthermore, it is known that the OCP measured during sliding action is a mixed potential which reflects the electrochemical state of the material outside (unworn) and inside (worn) the wear track (Ponthiaux et al., 2004). In this light, during the first 100 s of SLIDING 1 it seems that the electrochemical state of NT samples in the sliding contact area is kept unaltered, probably because TiO_2 NTs are able to withstand the mechanical actions and protect the underlying Ti substrate from AS. The gradual lowering of the OCP after this time suggests that the film is progressively degraded as sliding occurs. The COF monitored during this period indicates that the alumina ball is rubbing against an oxide film since 0.66 – 0.67 are typical COF values for alumina/Ti oxide tribological pair. Similar COF values comprised between 0.6 and 0.8 have been reported for sliding tests carried out on oxidized Ti surfaces against alumina ball (Alves et al., 2014, 2015, 2013). When SLIDING 2 starts the OCP begins decreasing gradually and, once it is finished, it increasingly evolves to noble values, and interestingly it follows similar depassivation and repassivation rates of the ones registered during and after SLIDING 1, respectively. Although the COF during SLIDING 2 tends to decrease, it still indicates that an oxide film is present in the contact region, whose presence is

confirmed by observation of the SEM BSE images of the wear scar remaining on NT samples (Fig. 3a and Fig. 4b). From these images it is observed that after two-cycle sliding a huge amount of NT film has been completely detached from the periphery of the contact area, revealing the poor adhesion strength of TiO_2 nanotubes. On the other hand, the formation of a compact oxide film is observed in the central region, where the sliding contact took place. As discovered in our previous study (Alves et al., 2017c), the NT film is catastrophically degraded within the first 100 – 300 s of SLIDING 1, during which the formation of a compact oxide film takes place as a result of the continuous smashing/densification of the film debris as long as mechanical solicitations take place. This tribofilm possesses the ability to protect the substrate against mechanical wear and also corrosion, therefore explaining the gradual lowering of the OCP during the first cycle of sliding. Based on this knowledge it is presumed that the gradual decrease of the OCP during SLIDING 1 and SLIDING 2 is being influenced by the formation of this tribofilm. As Vieira et al. (2012) highlighted, this may initiate a galvanic coupling in the wear track between depassivated and still passive areas and strongly influence the evolution of the potential during tribocorrosion. This tribofilm is probably granting the stable electrochemical features of NT samples when submitted to multiple mechanical actions, as observed from the similar depassivation and repassivation rates for both cycles of sliding.

Both NT-Ca/P/Zn samples show similar OCP values before mechanical solicitations (Fig. 2a – green and blue curves), and these are significantly higher compared to NT samples. The higher OCP reveals that TiO_2 NTs display a less active electrochemical state after bio-functionalization. This may be related with the fast and effective passivation ability of these samples immersed in AS, as previously deduced from potentiodynamic polarization studies of NT samples after bio-functionalization through the same methodology used in this study (Alves et al., 2017a). The improved electrochemical performance of bio-functionalized NTs is believed to be related with the formation of a nano-thick oxide film at the interface between Ti and TiO_2 NTs as observed in Fig. 1d, as a consequence of anodization process. As recently explained in a previous study of our group (Alves et al., 2017b), the Ti^{4+} ions released from the Ti substrate at the moment of anodic polarization, react with O^{2-} ions moving in opposite direction under the action of the electric field, leading to the formation of the Ti oxide film at the interface. As soon as mechanical solicitations start on NT-Ca/P/Zn#1 samples the OCP shifts down probably due to the wear of the topmost layers of the nanotubular film and after around 800 s, a more abrupt OCP fall takes place that may be related with the degradation of the film and exposure of the substrate to the harsh environment provided by AS. Immediately after the end of SLIDING 1, the OCP quickly recovers to higher values at a faster repassivation rate compared to NT samples, which highlights their ability of repassivation and the re-establishment of a noble potential close to the one attained during the first 800 s of sliding. During SLIDING 2, a different behavior is observed: the OCP slowly shifts down for around 1000 s, and afterwards it starts to evolve to values increasingly high towards the one achieved before sliding. Simultaneously to this noble evolution of the OCP, it is observed a decrease in the COF (Fig. 2c – green curve). This behavior suggests that repassivation of the wear track may be related with the formation of a tribofilm in the contact area with lubricant properties. To further investigate this phenomenon, additional BSE SEM images were taken in the wear tracks of both NT and NT-Ca/P/Zn samples, however, before cleaning procedure. In this way, additional information on the morphological and chemical features of the scar region in direct contact with alumina counterbody could be obtained. These images are shown in Fig. 6a and b for NT and NT-Ca/P/Zn samples, respectively. In the central region of the wear tracks remaining on NT and NT-Ca/P/Zn samples the presence of compacted mixed oxide films were found with a smooth appearance, contrasting with less oxidized regions from where most of the film has been probably detached. From observation of Fig. 6a and EDS spectra extracted from regions A1 and A2 indicated in the figure, it is observed that the tribofilm formed is characterized by a significantly higher at% of P. The presence of a P-rich tribofilm is also found on NT-Ca/P/Zn samples as observed from Fig. 6b and the correspondent EDS spectra in areas A1 and A2. The P-rich film on NT-Ca/P/Zn samples is additionally composed by Zn and a higher at% of Ca as a result of their bio-functionalization with these elements.

In this study, the formation of a P-rich tribofilm was observed during mechanical solicitations on TiO_2 nanotubular samples immersed in artificial saliva, which has phosphate ions (PO_4^{3-}) on its constitution. In fact, Hanawa and Ota (1991) reported that calcium phosphate is naturally formed on Ti surface immersed in a electrolyte solution containing inorganic ions found in biofluid, and approximately 60% of the phosphate was present as PO_4^{3-}. The authors explained that the formation of a calcium phosphate layer on Ti surface was firstly dictated by the adsorption of hydrated phosphate ions to Ti. Furthermore, previous studies have already demonstrated the ability of anodic Ti oxide films to induce the formation of apatite when immersed in simulated body fluids (Yang et al., 2004; Cui et al., 2009). The adsorption of negatively charged phosphate groups may be also mediated by the presence of Ca^{2+} ions in AS medium. As reported by Ribeiro et al. (2016), the negatively charged OH^- groups adsorbed to TiO_2 may be combined with the positively charged Ca^{2+} ions through electrostatic forces, subsequently combining with PO_4^{3-} ions. Therefore, the physicochemical properties of bio-functionalized TiO_2 NTs might influence the formation of the tribofilm, since these nanotubular structures also have Ca on their constitution. Based on this knowledge, it is expected that as soon as NT-Ca/P/Zn samples are immersed in AS, PO_4^{3-} ions in solution adsorb on TiO_2 NTs surface. Furthermore, once mechanical actions start and film degradation takes place, it is predictable that PO_4^{3-} ions in solution also adsorb on TiO_2 film debris, as illustrated in Fig. 7a. As long as sliding actions go on it is expected that the wear debris in the contact region are continuously submitted to complex mechanical and electrochemical solicitations, during which film debris become entrapped in the contact region and are continuously smashed and compacted. Consequently, these actions possibly induced the formation of the P-rich tribofilm in some regions of the wear track, most likely in those where the nanotubular film is thicker, as schematically illustrated in Fig. 7b.

In the present work, the formation of the P-rich tribofilm is being reflected in the increase of the OCP for NT-Ca/P/Zn#1 samples after 1000 s of SLIDING 2, and the simultaneous COF decrease (Fig. 2a and c – green curves). It is known that phosphate groups may act as lubricants (Yang et al., 2016), reducing the frictional force resisting to the relative sliding movement between neighboring surfaces, which is transduced in a lower COF. Furthermore, under wear action, PO_4^{3-} ions are known to undergo favorable reactions resulting in protective tribofilms (Somers et al., 2013; Dai et al., 2016). This might explain the smoothening effect observed on the surface of the tribofilm. However, the underlying mechanisms providing lubricant properties to this film still remain unclear and should be investigated in future studies. Although not so evident for NT surfaces, a small trend is also observed for a gradual decrease in the COF during SLIDING 2 (Fig. 2c – black curve) and the formation of this P-rich film may also be a reasonable explanation for that. On the other hand, another possibility is that once TiO_2 nanotubular film has undergone severe detachment, the alumina ball could be also in contact with the Ti substrate, a tribological pair that has a COF value of around 0.45 (Alves et al., 2013).

Even though the OCP values measured during two-cycle sliding tests have been different for NT-Ca/P/Zn#1 and NT-Ca/P/Zn#2 samples, the trend of OCP evolution was found quite similar between both, during mechanical solicitations (Fig. 2a – green and blue curves). In both cases two steady-states were achieved during SLIDING 1 at different OCP values, and at different time periods. Although during SLIDING 2 the OCP decreased only a few millivolts for NT-Ca/P/Zn#2 samples, the trend for COF decrease after 1000 s is similar to NT-Ca/P/

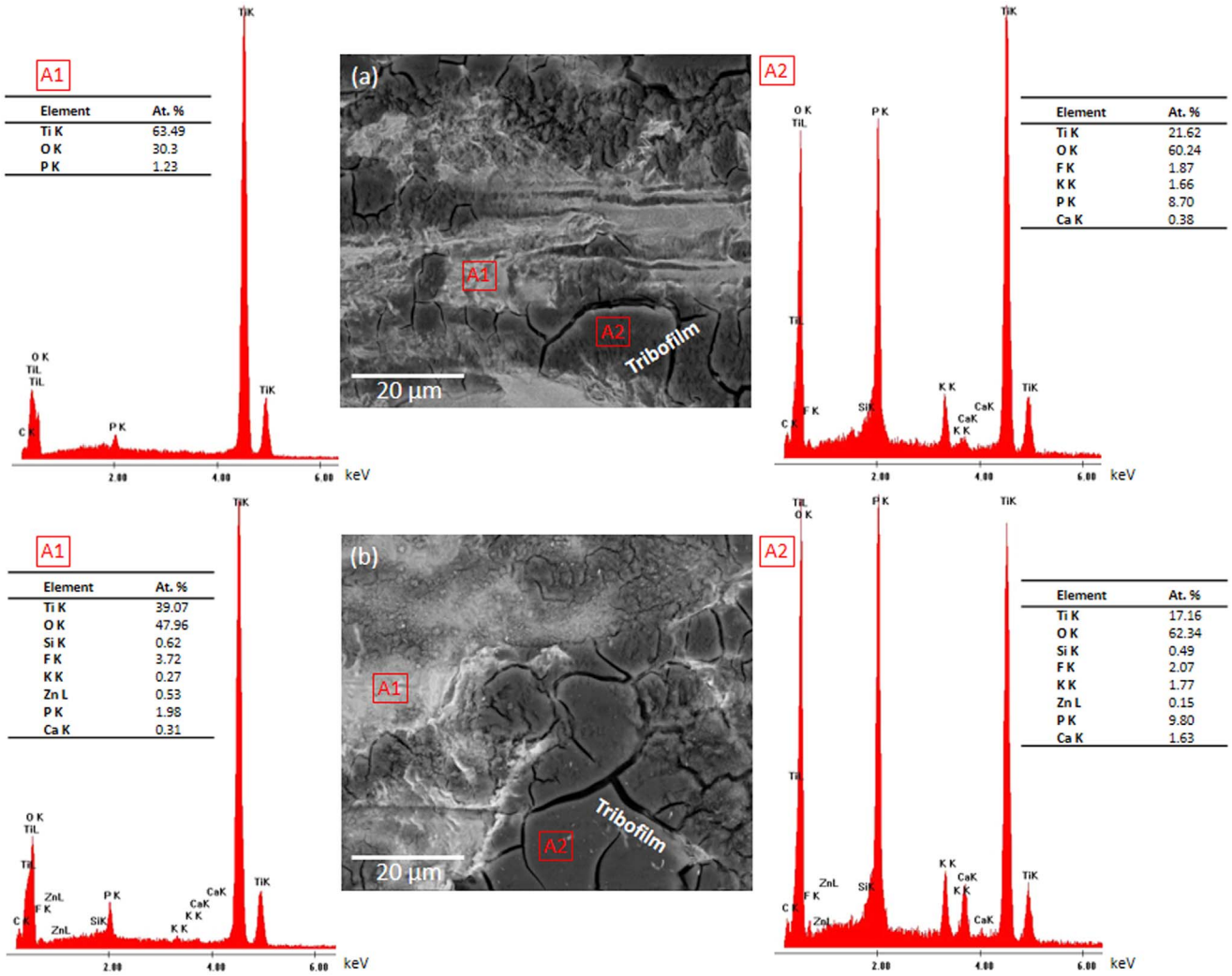

Fig. 6. BSE SEM micrographs in the central region of the wear tracks of (a) NT and (b) NT-Ca/P/Zn samples. The EDS spectra acquired from the inset red squares (A1 and A2) are depicted for both groups along with the insertion of the elemental composition and the atomic percentage (at%) of the detected elements.

Zn#1 samples (Fig. 2c – green and blue curves). No significant differences were found in the wear volume loss measured between NT-Ca/P/Zn#1 and NT-Ca/P/Zn#2 samples (Fig. 5), and therefore the differences in the OCP between both seem not be related with the level of mechanical damage of the nanotubular films. Most probably, the experimental conditions used for reciprocating sliding tests are close to the threshold conditions for NTs withstand mechanical solicitations without failure, which is dependent on their mechanical properties. Furthermore, the OCP might be also influenced by the total extension and thickness of the tribofilm formed, which may be thinner or thicker as the OCP is lower or higher, respectively. It is noteworthy to highlight that the OCP fluctuations observed during two-cycle sliding tests for both NT-Ca/P/Zn samples, might be related with Zn^{2+} ions liberation that have standard potential of -0.762 V *vs.* NHE (Zn^{2+}/Zn) (Delahay et al., 1951).

The wear volume loss was found significantly higher for NT than for both NT-Ca/P/Zn samples (Fig. 5). These differences may be related with the different adhesion strength of NT and NT-Ca/P/Zn films to the substrate, which seems be significantly higher for the latter. This is demonstrated by the lower mechanical damage observed for NT-Ca/P/Zn samples (Fig. 3), in parallel with their significantly reduced wear volume loss (Fig. 5). No detachment is observed in the area outside the contact region for these samples and the survival of NTs is found even in the border and central regions of their wear tracks (Fig. 4c and d). As a consequence of bio-functionalization of TiO_2 NTs and the formation of a nano-thick oxide film at the interface, the interfacial bonding to the substrate increased, and consequently their ability to withstand both electrochemical and mechanical solicitations, possibly by minimizing initiation and propagation of cracks. In the case of the bio-functionalized TiO_2 NTs, it is believed that the formation of the tribofilm during mechanical solicitations might be promoted by their improved wear resistance, since this may influence the extent of the chemical, electrochemical and mechanical interactions taking place in the contact region. These results are in good agreement with the findings reported in our previous work, in which bio-functionalized TiO_2 nanotubular films were exposed to one-cycle sliding tests for 300 s and 1800 s (Alves et al., 2017c). In this preceding study, a first insight on the main degradation mechanisms of TiO_2 nanotubular films was proposed which relies on tube smashing and densification, accompanied by delamination and detachment of the tubes, though cracks formation and propagation from the surface to subsurface regions of the film. After one-cycle sliding tests, severe plastic deformation and ploughing lines aligned in the direction of the counterbody movement were found showing evidences of abrasion, as well as material transfer from the materials surface to the alumina ball, *i.e.* adhesion wear. In the current work, when submitted to the second cycle of mechanical solicitations, abrasion grooves are still observed for all the samples along with plastic deformation (Fig. 3 and Fig. 6).

The formation of the tribofilm during tribo-electrochemical solicitations may help to explain the OCP evolution during sliding, both for

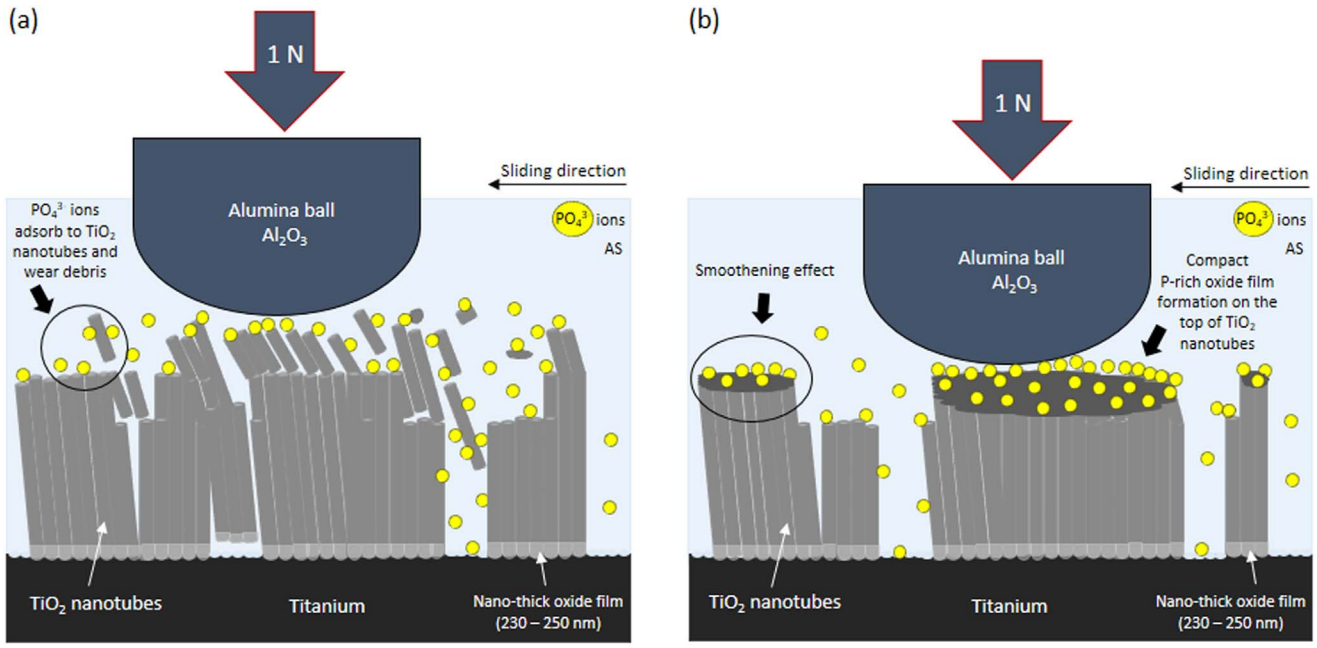

Fig. 7. Illustration of the possible formation mechanisms of the P-rich tribofilm during mechanical solicitations on bio-functionalized TiO_2 NTs immersed in AS. Firstly, PO_4^{3-} ions in the medium tend to adsorb to TiO_2 NTs and wear debris generated during sliding as shown in (a) and then, as the tribocorrosion interactions take place there is the formation of a compact P-rich oxide film on the top of bio-functionalized TiO_2 NTs as depicted in (b). The smoothening effect observed on the surface of the film is probable related with the lubricant properties of the film.

conventional and bio-functionalized TiO_2 NTs, as well as the high electrochemical stability observed in both cases when submitted to two-cycle sliding actions. Besides the improved electrochemical properties, the formation of the tribofilm is believed to synergistically improve the wear resistance ability of TiO_2 NTs. From our previous work (Alves et al., 2017c), conventional NTs showed similar degradation by mechanical wear after one-cycle sliding tests carried out for 300 s and 1800 s, while the present work shows that this trend was kept after two-cycle sliding periods undertaken for 1800 s each. As concerns bio-functionalized NTs, our previous work (Alves et al., 2017c) explains that a trend of a gradual degradation was observed for one-cycle sliding tests carried out for 300 s and 1800 s. Interestingly, the current investigation demonstrates that after two-cycle sliding periods, the mechanical wear degradation of bio-functionalized nanotubular films was kept in the same level as at the end of one-cycle 1800 s sliding tests. Therefore, the current findings highlight the ability of nanotubular films to withstand multiple cycles of mechanical solicitations, and suggest that the degradation induced by mechanical wear in the beginning of sliding action, dictate their long-term degradation. This ability of nanotubular films to avoid further mechanical degradation as long as mechanical solicitations take place, is believed to be strongly related with the formation of the compact P-rich tribofilm, which grants both protection against corrosion and wear.

4.2. Mechanical properties of TiO_2 NTs: significance and impact on wear resistance

The design of new implant systems with excellent mechanical properties is a requirement for long-term implant success. After bio-functionalization treatments the hardness of TiO_2 nanotubular films became significantly higher as compared to conventional TiO_2 NTs (Table 2). The hardness values for NT and NT-Ca/P/Zn samples were measured as 0.58 ± 0.08 GPa and 0.89 ± 0.15 GPa, respectively. Xu et al. (2015) also used nanoindentation to study the mechanical behavior of TiO_2 nanotube arrays, and their reported intrinsic hardness value was of 0.094 GPa. Yaghoubi et al. (2010) studied the mechanical properties of granular TiO_2 thin films by nanoindentation and reported hardness values increasing from 0.42 ± 0.05 GPa to 0.69 ± 0.05 GPa as annealing temperature increased from 100° to 300°C. These reported results are in the same order as our results. This improvement may be related with the nano-thick oxide film formed at the interface Ti/TiO_2 NTs after anodization treatments in the Ca/P/Zn-based electrolyte. The growth of this film at the interface improved the adhesion strength of TiO_2 NTs to the substrate, as previously deduced from the different tribocorrosion responses observed between NT and NT-Ca/P/Zn samples. It has been previously reported that the hardness is dependent on the film adhesion properties to the substrate, in such a way that as higher the adhesion strength higher the hardness (Stone et al., 1988; Azadmanjiri et al., 2016). A film with good adhesion to the substrate will constrain its plastic flow making the indentation more difficult that is transduced in a higher hardness than the one with poor adhesion (Stone et al., 1988; LaFontaine et al., 1990). This is also in good agreement with the significantly reduced wear loss in NT-Ca/P/Zn samples when compared to NT samples (Fig. 5), since a higher hardness is generally correlated with an improved wear resistance (Marques et al., 2016; Alves et al., 2013; Karthikeyan and Vijayaraghavan, 2016; Oliveira et al., 2015). Once NT-Ca/P/Zn films display improved adhesion properties to the substrate, consequently they display an improved ability to resist to mechanical wear.

Our results show that the hardness and elastic modulus of Ti surfaces are 2.58 ± 0.12 GPa and 127.25 ± 5.80 respectively. These are in agreement with Soares et al. (2008) who measured the hardness and elastic modulus of Ti polished surfaces by nanoindentation as 2.6 ± 0.7 GPa and 143 ± 23 GPa, respectively. In our work, the elastic modulus of TiO_2 NTs was significantly lower (around 63%) than that of Ti and was comprised between 42 and 52 GPa, both for NT and NT-Ca/P/Zn samples (Table 2). Existing literature describes elastic modulus of TiO_2 nanotube arrays ranging from 4 to 43 GPa (Crawford et al., 2009, 2007; Tang and Li, 2009). Our results are in accordance with the study performed by Crawford et al. (2007), who used nanoindentation and reported an elastic modulus for TiO_2 NTs of approximately 36 – 43 GPa, also found significantly lower than that of the Ti substrate. Furthermore, the calculated elastic modulus values are also in close agreement with the ones reported by Shokuhfar et al. (2009) who made direct

compressive measurements of individual TiO_2 NTs. The authors found that the elastic modulus of TiO_2 NTs depended on the diameter and wall thickness, and reported values in the range of 23–44 GPa. This range of values is lower when compared to that of dense amorphous TiO_2 of around 130–150 GPa (Crawford et al., 2007). This reduction may be related with the porous structure of TiO_2 nanotubular films, since it is known that the modulus of ceramic materials decreases with increasing porosity (Crawford et al., 2007). TiO_2 nanotubular surfaces display an elastic modulus approaching that of natural bone, which is around 11–30 GPa (Rho et al., 1997). Therefore, these surfaces are expected to have improved biomechanical compatibility than pure Ti, by reducing stress shielding effect (Mohseni et al., 2014) which is very well known to induce bone resorption at implant bone interface.

5. Limitations of the current study

As an innovative study in the field of tribocorrosion of dental implant materials, it faced some limitations that must be surpassed in the future. In this work, only OCP measurements were carried out and therefore no information on the rate of corrosion reactions taking place during sliding tests is provided. Thus, further tests should be performed under potentiostatic conditions to quantify the corrosion current released during mechanical solicitations and better predict the degradation mechanisms of nanotubular films by tribocorrosion. Furthermore, the characteristics of the P-rich tribofilm formed as a consequence of mechanical solicitations applied on nanotubular surfaces in AS should be thoroughly analyzed. It would be important to investigate the morphological, topographical and chemical features along the cross-section of the tribofilm, and further understand the mechanisms through which it provides corrosion protection and mechanical wear resistance. Finally, an additional important study would be to understand the mechanisms underlying lubrication properties of the P-rich protective film.

6. Conclusions

The tribocorrosion performance of conventional and bio-functionalized TiO_2 NTs was investigated when submitted to two-cycle sliding actions in artificial saliva. Furthermore, the mechanical properties of those films were investigated and correlations were found with their tribocorrosion responses. The main conclusions are as follows:

- TiO_2 NTs display a highly stable tribocorrosion response when submitted to two-cycle sliding actions. Furthermore, after bio-functionalization treatments, the tribocorrosion behavior of TiO_2 NTs was significantly improved both from the electrochemical and mechanical wear point of view.
- Bio-functionalized TiO_2 NTs display an increased hardness due to the formation of a nano-thick oxide film at the interface region that improves the adhesion strength of the nanotubes to the Ti substrate, and consequently their mechanical wear resistance.
- When submitted to tribo-electrochemical solicitations in artificial saliva, the degradation of TiO_2 NTs induces to the formation of a protective P-rich tribofilm with lubricant properties, which grants both electrochemical protection and resistance to mechanical wear.
- The elastic modulus of TiO_2 NTs is significantly lower compared to that of smooth Ti, and close that of natural bone.

In brief, bio-functionalized TiO_2 NTs through reverse polarization anodization display an improved ability to withstand two cycles of sliding actions in artificial saliva. These show up as multifunctional surfaces, with potential to simultaneously provide corrosion protection, resistance to mechanical degradation and avoid bone resorption by reducing stress shielding effect. This study provides fundamental and new insights for the development of TiO_2 NTs in Ti surfaces with long-term biomechanical compatibility and stability towards the new generation of dental implants.

Acknowledgements

This work was supported by FCT with the reference project UID/EEA/04436/2013 and by FEDER funds through the COMPETE 2020 – Programa Operacional Competitividade e Internacionalização (POCI) with the reference project POCI-01–0145-FEDER-006941.

The authors also acknowledge the financial support from FCT by the doctoral grant (Ref. SFRH/BD/88517/2012), CAPES (Proc. 99999.008666/2014-08), CNPq (Proc. 490761/2013-5) and UNESP. Moreover, the authors are grateful to LABNANO/CBPF (Brazilian Center for Research in Physics) for all the support provided in electron microscopy analyses. Finally, Tolou Shokuhfar is also thankful to US National Science Foundation NSF-DMR CAREER award # 1564950.

References

Alves, A., Oliveira, F., Wenger, F., Ponthiaux, P., Celis, J.-P., Rocha, L., 2013. Tribocorrosion behaviour of anodic treated titanium surfaces intended for dental implants. J. Phys. D: Appl. Phys. 46, 404001.
Alves, S., Bayón, R., Igartua, A., Saénz de Viteri, V., Rocha, L., 2014. Tribocorrosion behaviour of anodic titanium oxide films produced by plasma electrolytic oxidation for dental implants. Lubr. Sci. 26, 500–513.
Alves, S., Bayón, R., de Viteri, V.S., Garcia, M., Igartua, A., Fernandes, M., Rocha, L., 2015. Tribocorrosion Behavior of Calcium-and Phosphorous-Enriched Titanium Oxide Films and Study of Osteoblast Interactions for Dental Implants. J. Bio- Tribo-Corros. 1, 1–21.
Alves, S.A., Patel, S.B., Sukotjo, C., Mathew, M.T., Filho, P.N., Celis, J.-P., Rocha, L.A., Shokuhfar, T., 2017a. Synthesis of calcium-phosphorous doped TiO2 nanotubes by anodization and reverse polarization: a promising strategy for an efficient biofunctional implant surface. Appl. Surf. Sci. 399, 682–701.
Alves, S.A., Rossi, A.L., Ribeiro, A.R., Werckmann, J., Celis, J.-P., Rocha, L.A., Shokuhfar, T., 2017b. A first insight on the bio-functionalization mechanisms of TiO 2 nanotubes with calcium, phosphorous and zinc by reverse polarization anodization. Surf. Coat. Technol. 324, 153–166.
Alves, S.A., Rossi, A.L., Ribeiro, A.R., Toptan, F., Pinto, A.M., Celis, J.-P., Shokuhfar, T., Rocha, L.A., 2017c. Tribo-electrochemical behavior of bio-functionalized TiO2 nanotubes in artificial saliva: understanding of degradation mechanisms. Wear 384–385, 28–42.
Arenas, M.A., Pérez-Jorge, C., Conde, A., Matykina, E., Hernández-López, J.M., Pérez-Tanoira, R., de Damborenea, J.J., Gómez-Barrena, E., Esteba, J., 2013. Doped TiO2 anodic layers of enhanced antibacterial properties. Colloids Surf. B: Biointerfaces 105, 106–112.
Azadmanjiri, J., Wang, J.Y., Berndt, C.C., Kapoor, A., Zhu, D.M., Ang, A.S.M., Srivastava, V.K., 2016. Tantalum-and Silver-doped Titanium Dioxide Nanosheets Film: Influence on Interfacial Bonding Structure and Hardness of the Surface System. Industrial & Engineering Chemistry Research.
Brammer, K.S., Oh, S., Cobb, C.J., Bjursten, L.M., van der Heyde, H., Jin, S., 2009. Improved bone-forming functionality on diameter-controlled TiO2 nanotube surface. Acta Biomater. 5, 3215–3223.
Buciumeanu, M., Araujo, A., Carvalho, O., Miranda, G., Souza, J., Silva, F., Henriques, B., 2017. Study of the tribocorrosion behaviour of Ti6Al4V–HA biocomposites. Tribology Int. 107, 77–84.
Budinski, K.G., 1991. Tribological properties of titanium alloys. Wear 151, 203–217.
Butt, A., Lucchiari, N.B., Royhman, D., Runa, M.J., Mathew, M.T., Sukotjo, C., Takoudis, C.G., 2015. Design, development, and testing of a compact tribocorrosion apparatus for biomedical applications. J. Bio- Tribo-Corros. 1, 4.
Chen, J., Rungsiyakull, C., Li, W., Chen, Y., Swain, M., Li, Q., 2013. Multiscale design of surface morphological gradient for osseointegration. J. Mech. Behav. Biomed. Mater. 20, 387–397.
Cobelli, N., Scharf, B., Crisi, G.M., Hardin, J., Santambrogio, L., 2011. Mediators of the inflammatory response to joint replacement devices. Nat. Rev. Rheumatol. 7, 600–608.
Crawford, G., Chawla, N., Das, K., Bose, S., Bandyopadhyay, A., 2007. Microstructure and deformation behavior of biocompatible TiO2 nanotubes on titanium substrate. Acta Biomater. 3, 359–367.
Crawford, G., Chawla, N., Houston, J., 2009. Nanomechanics of biocompatible TiO2 nanotubes by interfacial force microscopy (IFM). J. Mech. Behav. Biomed. Mater. 2, 580–587.
Cruz, H.V., Souza, J.C.M., Henriques, M., Rocha, L.A., 2011. Tribocorrosion and bio-tribocorrosion in the oral environment: the case of dental implants. In: David, J.P. (Ed.), Biomedical Tribology. Nova Science Publishers, pp. 1–30.
Cruz, H.V., Henriques, M., Teughels, W., Celis, J.-P., Rocha, L.A., 2015. Combined influence of fluoride and biofilms on the biotribocorrosion behavior of titanium used for dental applications. J. Bio- Tribo-Corros. 1, 1–12.
Cui, X., Kim, H.M., Kawashita, M., Wang, L., Xiong, T., Kokubo, T., Nakamura, T., 2009. Preparation of bioactive titania films on titanium metal via anodic oxidation. Dent. Mater. 25, 80–86.
Dai, W., Kheireddin, B., Gao, H., Kan, Y., Clearfield, A., Liang, H., 2016. Formation of anti-wear tribofilms via α-ZrP nanoplatelet as lubricant additives. Lubricants 4, 28.
Delahay, P., Pourbaix, M., Van Rysselberghe, P., 1951. Potential-pH diagram of zinc and its applications to the study of zinc corrosion. J. Electrochem. Soc. 98, 101–105.

Doni, Z., Alves, A., Toptan, F., Gomes, J., Ramalho, A., Buciumeanu, M., Palaghian, L., Silva, F., 2013. Dry sliding and tribocorrosion behaviour of hot pressed CoCrMo biomedical alloy as compared with the cast CoCrMo and Ti6Al4V alloys. Mater. Des. 52, 47–57.
Ercan, B., Taylor, E., Alpaslan, E., Webster, T.J., 2011. Diameter of titanium nanotubes influences anti-bacterial efficacy. Nanotechnology 22, 295102.
Fusayama, T., Katayori, T., Nomoto, S., 1963. Corrosion of gold and amalgam placed in contact with each other. J. Dent. Res. 42, 1183–1197.
Gao, A., Hang, R., Huang, X., Zhao, L., Zhang, X., Wang, L., Tang, B., Ma, S., Chu, P.K., 2014. The effects of titania nanotubes with embedded silver oxide nanoparticles on bacteria and osteoblasts. Biomaterials 35, 4223–4235.
Geringer, J., Macdonald, D.D., 2014. Friction/fretting-corrosion mechanisms: current trends and outlooks for implants. Mater. Lett. 134, 152–157.
Gulati, K., Aw, M.S., Losic, D., 2011. Drug-eluting Ti wires with titania nanotube arrays for bone fixation and reduced bone infection. Nanoscale Res. Lett. 6, 571.
Gulati, K., Ramakrishnan, S., Aw, M.S., Atkins, G.J., Findlay, D.M., Losic, D., 2012. Biocompatible polymer coating of titania nanotube arrays for improved drug elution and osteoblast adhesion. Acta Biomater. 8, 449–456.
Hacisalihoglu, I., Samancioglu, A., Yildiz, F., Purcek, G., Alsaran, A., 2015. Tribocorrosion properties of different type titanium alloys in simulated body fluid. Wear 332, 679–686.
Hanawa, T., Ota, M., 1991. Calcium phosphate naturally formed on titanium in electrolyte solution. Biomaterials 12, 767–774.
Holland, R., 1992. Corrosion testing by potentiodynamic polarization in various electrolytes. Dent. Mater. 8, 241–245.
Holmberg, K.V., Abdolhosseini, M., Li, Y., Chen, X., Gorr, S.-U., Aparicio, C., 2013. Bio-inspired stable antimicrobial peptide coatings for dental applications. Acta Biomater. 9, 8224–8231.
Hu, Y., Cai, K., Luo, Z., Xu, D., Xie, D., Huang, Y., Yang, W., Liu, P., 2012. TiO 2 nanotubes as drug nanoreservoirs for the regulation of mobility and differentiation of mesenchymal stem cells. Acta Biomater. 8, 439–448.
Ingham, E., Fisher, J., 2000. Biological reactions to wear debris in total joint replacement. Proc. Inst. Mech. Eng., Part H: J. Eng. Med. 214, 21–37.
Ingham, E., Fisher, J., 2005. The role of macrophages in osteolysis of total joint replacement. Biomaterials 26, 1271–1286.
Karthikeyan, S., Vijayaraghavan, L., 2016. Influence of nano Al2O3 particles on the adhesion, hardness and wear resistance of electroless NiP coatings. Int. J. Mater., Mech. Manuf. 4, 106–110.
Kodama, A., Bauer, S., Komatsu, A., Asoh, H., Ono, S., Schmuki, P., 2009. Bioactivation of titanium surfaces using coatings of TiO2 nanotubes rapidly pre-loaded with synthetic hydroxyapatite. Acta Biomater. 5, 2322–2330.
LaFontaine, W.R., Yost, B., Li, C.-Y., 1990. Effect of residual stress and adhesion on the hardness of copper films deposited on silicon. J. Mater. Res. 5, 776–783.
Liu, X., Chu, P.K., Ding, C., 2010. Surface nano-functionalization of biomaterials. Mater. Sci. Eng.: R: Rep. 70, 275–302.
Marques, Id.S.V., Alfaro, M.F., Da Cruz, N.C., Mesquita, M.F., Takoudis, C., Sukotjo, C., Mathew, M.T., Barão, V.A.R., 2016. Tribocorrosion behavior of biofunctional titanium oxide films produced by micro-arc oxidation: synergism and mechanisms. J. Mech. Behav. Biomed. Mater. 60, 8–21.
Mathew, M.T., Abbey, S., Hallab, N.J., Hall, D.J., Sukotjo, C., Wimmer, M.A., 2012. Influence of pH on the tribocorrosion behavior of CpTi in the oral environment: synergistic interactions of wear and corrosion. J. Biomed. Mater. Res. Part B: Appl. Biomater. 100, 1662–1671.
Mendonça, G., Mendonça, D.B.S., Simões, L.G.P., Araújo, A.L., Leite, E.R., Golin, A.L., Aragão, F.J.L., Cooper, L.F., 2011. Nanostructured implant surface effect on osteoblast gene expression and bone-to-implant contact in vivo. Mater. Sci. Eng.: C. 31, 1809–1818.
Miraghaei, S., Ashrafizadeh, F., Raeissi, K., Santamaria, M., Di Quarto, F., 2011. An electrochemical investigation on the adhesion of As-formed anodic TiO2 nanotubes grown in organic solvents. Electrochem. Solid-State Lett. 14, K8–K11.
Mohseni, E., Zalnezhad, E., Bushroa, A., 2014. Comparative investigation on the adhesion of hydroxyapatite coating on Ti–6Al–4V implant: a review paper. Int. J. Adhes. Adhes. 48, 238–257.
Oliveira, F.G., Ribeiro, A.R., Perez, G., Archanjo, B.S., Gouvea, C.P., Araújo, J.R., Campos, A.P., Kuznetsov, A., Almeida, C.M., et al., 2015. Understanding growth mechanisms and tribocorrosion behaviour of porous TiO 2 anodic films containing calcium, phosphorous and magnesium. Appl. Surf. Sci. 341, 1–12.
Oliver, W.C., Pharr, G.M., 1992. An improved technique for determining hardness and elastic modulus using load and displacement sensing indentation experiments. J. Mater. Res. 7, 1564–1583.
Olmedo, D.G., Paparella, M.L., Brandizzi, D., Cabrini, R.L., 2010. Reactive lesions of peri-implant mucosa associated with titanium dental implants: a report of 2 cases. Int. J. Oral. Maxillofac. Surg. 39, 503–507.
Ponthiaux, P., Wenger, F., Drees, D., Celis, J.-P., 2004. Electrochemical techniques for studying tribocorrosion processes. Wear 256, 459–468.
Popat, K.C., Leoni, L., Grimes, C.A., Desai, T.A., 2007a. Influence of engineered titania nanotubular surfaces on bone cells. Biomaterials 28, 3188–3197.
Popat, K.C., Eltgroth, M., LaTempa, T.J., Grimes, C.A., Desai, T.A., 2007b. Decreased Staphylococcus epidermis adhesion and increased osteoblast functionality on antibiotic-loaded titania nanotubes. Biomaterials 28, 4880–4888.
Puckett, S.D., Taylor, E., Raimondo, T., Webster, T.J., 2010. The relationship between the nanostructure of titanium surfaces and bacterial attachment. Biomaterials 31, 706–713.
Rho, J.-Y., Tsui, T.Y., Pharr, G.M., 1997. Elastic properties of human cortical and trabecular lamellar bone measured by nanoindentation. Biomaterials 18, 1325–1330.
Ribeiro, A.R., Gemini-Piperni, S., Travassos, R., Lemgruber, L., Silva, R.C., Rossi, A.L., Farina, M., Anselme, K., Shokuhfar, T., et al., 2016. Trojan-like internalization of anatase titanium dioxide nanoparticles by human osteoblast cells. Sci. Rep. 6.
Robin, A., Meirelis, J., 2007. Influence of fluoride concentration and pH on corrosion behavior of Ti-6Al-4V and Ti-23Ta alloys in artificial saliva. Mater. Corros. 58, 173–180.
Rocha, L., Oliveira, F., Cruz, H., Sukotjo, C., Mathew, M., 2013. Bio-Tribocorrosion in Biomaterials and Medical Implants, In Bio-tribocorrosion in Dental Applications. Elsevier Inc, pp. 223–249.
Rodrigues, T., Moreira, F., Guerra, F., Nicolau, P., Neto, M.A., 2014. Clinical trial—in vivo endosseous implants micromovements measuring with 3D digital image Correlation method. Biodental Eng. III 77.
Runa, M., Mathew, M., Rocha, L., 2013. Tribocorrosion response of the Ti6Al4V alloys commonly used in femoral stems. Tribology Int. 68, 85–93.
Sampaio, M., Buciumeanu, M., Henriques, B., Silva, F.S., Souza, J.C., Gomes, J.R., 2016. Tribocorrosion behavior of veneering biomedical PEEK to Ti6Al4V structures. J. Mech. Behav. Biomed. Mater. 54, 123–130.
Shokuhfar, T., Arumugam, G.K., Heiden, P.A., Yassar, R.S., Friedrich, C., 2009. Direct compressive measurements of individual titanium dioxide nanotubes. ACS nano 3, 3098–3102.
Shokuhfar, T., Sinha-Ray, S., Sukotjo, C., Yarin, A.L., 2013. Intercalation of anti-inflammatory drug molecules within TiO 2 nanotubes. RSC Adv. 3, 17380–17386.
Shokuhfar, T., Hamlekhan, A., Chang, J.-Y., Choi, C.K., Sukotjo, C., Friedrich, C., 2014. Biophysical evaluation of cells on nanotubular surfaces: the effects of atomic ordering and chemistry. Int. J. Nanomed. 9, 3737.
Sivakumar, B., Kumar, S., Narayanan, T.S., 2011. Fretting corrosion behaviour of Ti–6Al–4V alloy in artificial saliva containing varying concentrations of fluoride ions. Wear 270, 317–324.
Soares, P., Mikowski, A., Lepienski, C.M., Santos, E., Soares, G.A., Kuromoto, N.K., 2008. Hardness and elastic modulus of TiO2 anodic films measured by instrumented indentation. J. Biomed. Mater. Res. Part B: Appl. Biomater. 84, 524–530.
Somers, A.E., Howlett, P.C., MacFarlane, D.R., Forsyth, M., 2013. A review of ionic liquid lubricants. Lubricants 1, 3–21.
Souza, J., Barbosa, S., Ariza, E., Celis, J.-P., Rocha, L., 2012. Simultaneous degradation by corrosion and wear of titanium in artificial saliva containing fluorides. Wear 292, 82–88.
Souza, J.C., Barbosa, S.L., Ariza, E.A., Henriques, M., Teughels, W., Ponthiaux, P., Celis, J.-P., Rocha, L.A., 2015. How do titanium and Ti6Al4V corrode in fluoridated medium as found in the oral cavity? An in vitro study. Mater. Sci. Eng.: C 47, 384–393.
Stone, D., LaFontaine, W.R., Alexopoulos, P., Wu, T.W., Li, C.-Y., 1988. An investigation of hardness and adhesion of sputter-deposited aluminum on silicon by utilizing a continuous indentation test. J. Mater. Res. 3, 141–147.
Szmukler-Moncler, S., Salama, H., Reingewirtz, Y., Dubruille, J.H., 1998. Timing of loading and effect of micromotion on bone-dental implant interface: review of experimental literature. J. Biomed. Mater. Res. 43, 192–203.
Tang, X., Li, D., 2009. Fabrication, geometry, and mechanical properties of highly ordered TiO2 nanotubular arrays. J. Phys. Chem. C 113, 7107–7113.
Tomsia, A.P., Launey, M.E., Lee, J.S., Mankani, M.H., Wegst, U.G., Saiz, E., 2011. Nanotechnology approaches for better dental implants. Int. J. Oral. Maxillofac. Implants 26, 25.
Toptan, F., Rego, A., Alves, A., Guedes, A., 2016. Corrosion and tribocorrosion behavior of Ti–B 4C composite intended for orthopaedic implants. J. Mech. Behav. Biomed. Mater. 61, 152–163.
Toptan, F., Alves, A., Pinto, A., Ponthiaux, P., 2017. Tribocorrosion behavior of biofunctionalized highly porous titanium. J. Mech. Behav. Biomed. Mater. 69, 144–152.
Vasilev, K., Poh, Z., Kant, K., Chan, J., Michelmore, A., Losic, D., 2010. Tailoring the surface functionalities of titania nanotube arrays. Biomaterials 31, 532–540.
Vieira, A., Rocha, L., Papageorgiou, N., Mischler, S., 2012. Mechanical and electrochemical deterioration mechanisms in the tribocorrosion of Al alloys in NaCl and in nano 3 solutions. Corros. Sci. 54, 26–35.
Villanueva, J., Trino, L., Thomas, J., Bijukumar, D., Royhman, D., Stack, M., 2017. and Mathew M. corrosion, tribology, and tribocorrosion research in biomedical implants: progressive trend in the published literature. J. Bio- Tribo-Corros. 3, 1.
Xu, Y., Liu, M., Wang, M., Oloyede, A., Bell, J., Yan, C., 2015. Nanoindentation study of the mechanical behavior of TiO2 nanotube arrays. J. Appl. Phys. 118, 145301.
Yaghoubi, H., Taghavinia, N., Alamdari, E.K., Volinsky, A.A., 2010. Nanomechanical properties of TiO2 granular thin films. ACS Appl. Mater. Interfaces 2, 2629–2636.
Yang, B., Uchida, M., Kim, H.-M., Zhang, X., Kokubo, T., 2004. Preparation of bioactive titanium metal via anodic oxidation treatment. Biomaterials 25, 1003–1010.
Yang, Y., Zhang, C., Wang, Y., Dai, Y., Luo, J., 2016. Friction and wear performance of titanium alloy against tungsten carbide lubricated with phosphate ester. Tribol. Int. 95, 27–34.
Yazici, H., Fong, H., Wilson, B., Oren, E.E., Amos, F.A., Zhang, H., Evans, J.S., Snead, M.L., Sarikaya, M., et al., 2013. Biological response on a titanium implant-grade surface functionalized with modular peptides. Acta Biomater. 9, 5341–5352.
Yu, D., Zhu, X., Xu, Z., Zhong, X., Gui, Q., Song, Y., Zhang, S., Chen, X., Li, D., 2014. Facile method to enhance the adhesion of TiO2 nanotube arrays to Ti substrate. ACS Appl. Mater. Interfaces 6, 8001–8005.
Zhang, W., Wang, G., Liu, Y., Zhao, X., Zou, D., Zhu, C., Jin, Y., Huang, Q., Sun, J., et al., 2013. The synergistic effect of hierarchical micro/nano-topography and bioactive ions for enhanced osseointegration. Biomaterials 34, 3184–3195.
Zhao, L., Mei, S., Chu, P.K., Zhang, Y., Wu, Z., 2010. The influence of hierarchical hybrid micro/nano-textured titanium surface with titania nanotubes on osteoblast functions. Biomaterials 31, 5072–5082.
Zhao, L., Wang, H., Huo, K., Cui, L., Zhang, W., Ni, H., Zhang, Y., Wu, Z., Chu, P.K., 2011. Antibacterial nano-structured titania coating incorporated with silver nanoparticles. Biomaterials 32, 5706–5716.
Zhao, M., Li, J., Li, Y., Wang, J., Zuo, Y., Jiang, J., Wang, H., 2014. Gradient control of the adhesive force between Ti/TiO2 nanotubular arrays fabricated by anodization. Sci. Rep. 4.